IEEE Access
Multidisciplinary | Rapid Review | Open Access Journal

IEEE VEHICULAR TECHNOLOGY SOCIETY SECTION

Received 20 April 2023, accepted 29 May 2023, date of publication 2 June 2023, date of current version 13 June 2023.

Digital Object Identifier 10.1109/ACCESS.2023.3282253

RESEARCH ARTICLE

Embedded Inertial Sensor-Based Road to Vehicle Pitch Estimation for Automatic Headlamp Leveling

CHANSOO KIM[1], JIWON SEOK[1], SOYEONG KIM[1], KUNHO LEE[2], JONGHWA KIM[2], INSUB MOON[2], JISUNG KANG[2], AND KICHUN JO[1], (Member, IEEE)

[1]Department of Smart Vehicle Engineering, Konkuk University, Gwangjin-gu, Seoul 05029, Republic of Korea
[2]Headlamp Electronic Engineering Team, Hyundai Mobis Company, Seoul, Gyeonggi-do 16891, South Korea

Corresponding author: Kichun Jo (kichun@konkuk.ac.kr)

This work was supported in part by Hyundai Mobis Company Headlamp Electronic Engineering Team, Gyeonggi-do, Republic of Korea; in part by the National Research Foundation of Korea (NRF) Grant funded by the Korea Government (MSIT) under Grant RS-2023-00209252; and in part by the Korea Institute for Advancement of Technology (KIAT) Grant funded by the Korea Government (MOTIE) (HRD Program for Industrial Innovation) under Grant P0020536.

ABSTRACT The irradiation angle of the headlights is regulated by the United Nations Economic Commission for Europe (UNECE) for safe driving by preventing glare from oncoming drivers. Automatic headlamp leveling is a system that automatically controls the angle of the headlamp horizontally to meet safety regulations. To control the irradiation angle, the automatic headlamp leveling system must estimate the road-to-headlamp pitch angle. This paper proposes an accurate and robust road-to-headlamp pitch angle estimation system using a low-cost MEMS (Micro Electro Mechanical Systems) IMU (Inertial Measurement Unit) sensor. The proposed system sequentially estimates the headlamp pitch angle, the road slope angle, and the road-to-headlamp pitch angle. First, headlamp pitch angle is estimated using the gravity from IMU. Second, the road slope angle is estimated based on vehicle prior knowledge that the vehicle is moving in the direction of the road. Finally, road-to-headlamp pitch angle is estimated by subtracting road slope angle from headlamp pitch angle. However, the measurement data of a MEMS IMU sensor contains various types of noise, such as bias and white noise. For that reason, reducing the effects of MEMS IMU noise is highly important when estimating the road-to-headlamp pitch angle. Therefore, the proposed system focuses on minimizing the effects of the low-cost MEMS IMU noise. In addition, the proposed method is verified by simulations and experiments. The simulation analyzes the effect of the MEMS IMU sensor noise on the estimation accuracy and precision. Finally, the proposed algorithm shows more robust and accurate performance compared with other methods on the test and common road verifications.

INDEX TERMS Automatic headlamp leveling, inertial measurement unit (IMU), road to headlamp pitch angle estimation, road slope estimation.

I. INTRODUCTION

The vehicle headlamp is essential for lightening the ego vehicle's foresight in darkness. Recently, most headlamps provide long visibility distances and high luminous intensity because of the technological development of Light Emitting Diode (LED) and High-Intensity Discharge (HID). As shown in Fig. 1, when the irradiation angle of the headlamp is too high, a vehicle accident may occur due to the glare of an oncoming vehicle driver. For that reason, the irradiation angle of the headlamp is regulated for all vehicles not to exceed the horizontal line through United Nations Economic Commission for Europe (UNECE) [1]. The challenge is that the irradiation angle of the headlamps must be adjusted when the weight of the load on the vehicle changes.

The associate editor coordinating the review of this manuscript and approving it for publication was Jie Gao.

This work is licensed under a Creative Commons Attribution-NonCommercial-NoDerivatives 4.0 License.
For more information, see https://creativecommons.org/licenses/by-nc-nd/4.0/

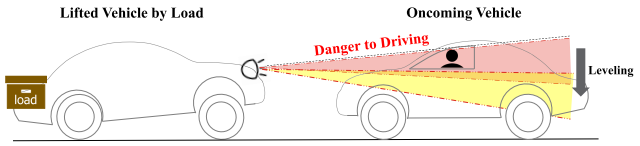

FIGURE 1. The irradiation angle of the headlamp is raised by the load, and the raised light interrupts the sight of oncoming drivers. Headlamp leveling is to lower the raised angle of irradiation to improve safety.

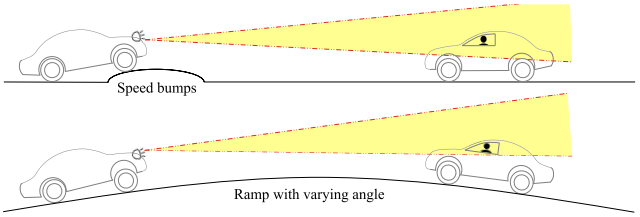

FIGURE 2. In this paper, it is a non-covered scenario and is not included in the scope of UNECE regulation. It can be implemented only when both the fast actuator and forward recognition sensor are attached.

There are two types of headlamp leveling: manual headlamp leveling and automatic headlamp leveling. Manual headlamp leveling requires drivers to operate the headlamp level manually, which degrades drivers' convenience and safety. On the other hand, automatic leveling is a system that automatically adjusts the angle of the headlamp, contributing greatly to convenience and driver safety. Automatic leveling is divided into static leveling and dynamic leveling. Static leveling is to control the irradiation angle of the headlamp by estimating the pitch change by various loading conditions. As shown in Fig. 2, Dynamic leveling controls the irradiation angle immediately as the vehicle pitch changes by a speed bump or ramps with varying angles [2], [3]. In dynamic leveling, not only the road-to-pitch angle but also the shape information of the road in front of the vehicle is additionally required as shown in Fig. 2. For dynamic leveling to be implemented, expensive high-speed actuators and forward perception sensors such as cameras or LiDARs (Light Detection and Ranging) are required. Therefore, when using only height sensors and IMU that can estimate the road-to-headlamp pitch angle, scenarios of speed bumps or ramps with varying angles are not possible [4], [5].

For automatic headlamp leveling, the road-to-headlamp pitch angle must be estimated. Typically, there are several types of sensors to estimate the road-to-headlamp pitch angle, such as height sensors and Micro Electro Mechanical System (MEMS) Inertial Measurement Unit (IMU) sensors. The height sensors, which measure the height between the body frame and each wheel, can estimate the pitch angle using the difference between the front axle height and the rear axle height [3], [6]. This height sensor-based pitch estimation method is very straightforward. But installing the height sensor is expensive because the wire harness must be connected from the front and rear sensors to the auto-leveling computer. In addition, the height sensor is always placed in harsh environments near the wheels, which can cause durability issues.

A low-cost MEMS IMU-based road-to-headlamp pitch angle estimation system has been recently proposed to overcome this drawback. Low-cost MEMS IMU sensor can be easily attached to the headlamp Electric Controller Unit (ECU) board. Therefore, wiring harness to the rear axle is unnecessary, unlike the height sensor-based method. Also, there is no need to re-design the auto-leveling system when the vehicle model changes because the IMU can be installed inside the ECU, which can be reused for various vehicles.

However, to our best knowledge, there is no drift-free method for IMU-based headlamp leveling. Some methods recognize a vehicle's stationary state where load conditions may change, such as when a door or trunk opens [6]. When stopping, the road-to-IMU pitch angle is estimated by integrating the change amount of the IMU pitch angle [7]. However, the method of integrating the change of the IMU pitch causes drift error. To overcome this drift problem, a drift-free method of estimating the road-to-headlamp pitch angle is proposed. A real-time road-to-IMU pitch angle estimation method based on the Kalman filter has been proposed, but the experimental results are divergent and not suitable for static leveling [8]. A method for estimating the road-to-headlamp pitch angle in the direction of acceleration has also been proposed [9], [10]. This method assumes that the direction of acceleration is the road-to-IMU pitch angle. However, since the vehicle has pitch motion, the direction of acceleration is not the road-to-IMU angle. Also, since it is an algorithm that operates only on flat ground, it cannot be applied to a vehicle running on the ramp.

IMU-based road slope angle estimation methods have been proposed several times. Some papers do not differentiate between road slope angle and IMU pitch angle [11], [12]. These methods treat the IMU pitch angle and the road slope angle the same. It cannot be applied to automatic headlamp leveling that has to distinguish between road frame and IMU frame. A method for estimating the orientation of the acceleration as a road-to-IMU pitch angle was proposed [13], [14]. However, it is not suitable for the road slope estimation method for automatic headlamp leveling because the pitch motion of the vehicle is not considered under the assumption that the acceleration direction and the road slope direction are parallel. Additionally, this method includes many vehicle parameters, and tuning is required for each vehicle.

IMU-based pitch angle estimation methods have been proposed many time. There are two methods of estimating attitude (roll and pitch) using IMU. One is to use the gravity of the accelerometer, and the second is to integrate the gyroscope. The method using gravity accurately estimates the attitude when stationary, but when the vehicle moves, the estimation result becomes inaccurate due to external acceleration. The method of integrating the gyroscope can be used during motion, but drift error occurs because of the integration. Most IMU-based attitude estimation systems use these two methods by taking advantage of each method. Methods using both methods can be roughly divided into two types. First, the threshold-based switching method uses a

threshold to divide it into the static condition and dynamic condition [15], [16], [17], [18]. In static conditions without external acceleration, the gravity of the accelerometer is used, and during dynamic conditions, the attitude is estimated by integrating the gyroscope. In general, as the norm of accelerometer measurement is closer to 9.81 m/s^2, it is recognized as a static condition. This zero velocity detection methodology has been widely proposed under the name of Zero Velocity UpdaTe (ZUPT) [19], [20], [21]. When the static condition is recognized, the gyroscope bias can be removed with the information that the gyroscope should output zero [15]. The second is the sensor fusion method. The most common method is to fuse the accelerometer, and the gyroscope, which fuses the two tilt measurement information based on the tuning parameters called a complementary filter [22]. There is also a method of estimating attitude using gravity by estimating and eliminating external acceleration based on the gyroscope [23]. In addition, methods to estimate external acceleration by fusion of GPS and wheel speed sensor have been proposed [24].

This paper proposes a framework for estimating road-to-headlamp pitch angle using a low-cost MEMS IMU sensor for a static headlamp leveling system. The overall system consists of four parts. The first part is a calibration that removes the gyroscope bias that causes estimation errors. The second part estimates the IMU pitch angle when the vehicle stops. Third, the road slope angle is estimated using the estimated array of position data, which is predicted with an IMU-based dead-reckoning algorithm [25]. Finally, the road-to-IMU pitch angle can be obtained using the IMU pitch angle and road slope angle estimated in the above two steps. In addition, we analyze the effect of various IMU noises on this system and then verify the estimation performance with simulation and real vehicle experiments.

The contributions of this paper are as follows:

1) We propose a framework to estimate the road-to-headlamp pitch angle for automatic headlamp leveling using only MEMS IMU. The proposed system satisfies UNECE regulations by using a mass-produced IMU sensor with limited resources without an expensive height sensor.
2) The road slope angle estimation model is proposed based on the assumption that the vehicle moves in the road slope direction. Accurate estimation is possible using data that satisfies specific conditions to minimize the integration error and drift error of MEMS IMU sensors. In the road slope angle estimation model, the positions obtained from an existing IMU-based dead reckoning model are used.
3) The proposed system is verified in various cases through simulation, test road experiments, and common road experiments. The effect of the IMU sensor noise on the proposed system is analyzed through simulation, and each module is experimentally evaluated in the test road experiment. Finally, the proposed method shows state-of-the-art performance compared to other IMU-based methods in general road tests.

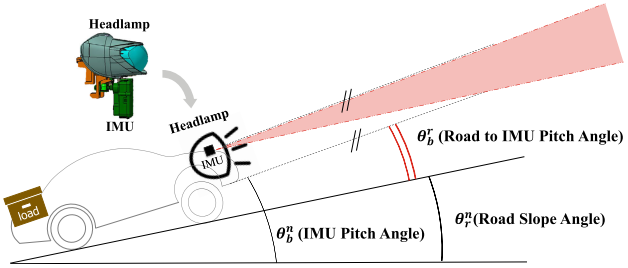

FIGURE 3. The IMU is attached to the headlamp and is aligned with the orientation of the headlamp. The angle required for headlamp leveling is the road-to-IMU pitch angle (θ_b^r) that is obtained by subtracting the road slope angle (θ_r^b) from the IMU pitch angle (θ_b^n).

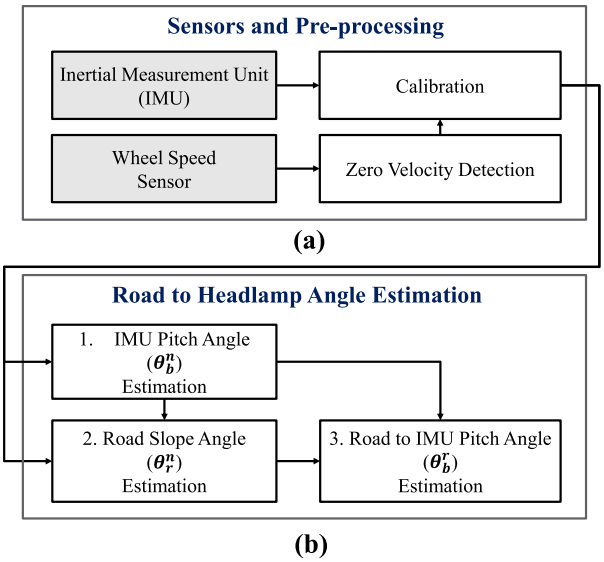

FIGURE 4. The proposed system consists of two parts. The first part (a) is sensor and pre-processing, and the second part (b) is the road to headlamp pitch angle estimation part.

The rest of this paper is organized as follows. Section II describes a system architecture. The coordinate system, notation, and sensor pre-processing are explained in section III. In section IV, the proposed algorithm is explained in detail. Section V describes the evaluation results, and we conclude the paper in the final section VI.

II. SYSTEM ARCHITECTURE

The purpose of the system is to estimate the road-to-IMU pitch angle (θ_b^r) as shown in Fig. 3. The road-to-IMU pitch angle is obtained by subtracting the road slope angle (θ_r^n) from the IMU pitch angle (θ_b^n), using (1). Therefore, the proposed system was also designed to sequentially estimate the IMU pitch angle, road slope angle, and road-to-IMU pitch angle. In static leveling, the road-to-IMU pitch angle is estimated as a constant if the load condition is not changed.

$$\theta_b^r = \theta_b^n - \theta_r^n \tag{1}$$

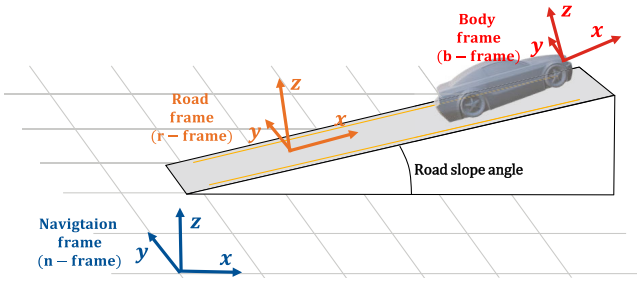

FIGURE 5. Navigation frame (n-frame): The x-y plane of the n-frame is perpendicular to gravity. The n-frame is stationary and does not move. The states of the IMU, such as position, velocity, and orientation, are defined in this frame. Road frame (r-frame): r-frame is a fixed frame like an n-frame. Unlike the n-frame, the z-axis of the r-frame is perpendicular to the road. Body frame (b-frame): The body frame is the IMU frame and headlamp frame. The body frame moves as the position of the IMU changes. IMU sensor measurements are measured in the b-frame.

The system architecture is mainly composed of two parts, as shown in Fig. 4. Fig. 4 (a) is the first part, sensors and pre-processing. Two sensors, IMU and wheel speed sensor, are modelled. Pre-processing consists of a calibration module and a zero velocity detection module. The calibration module removes the bias of the gyroscope, and the zero velocity detection module recognizes the information that the vehicle is in a stationary state. The second part consists of three modules, as shown in Fig. 4 (b): IMU pitch angle estimation, road slope estimation, and road-to-IMU pitch angle estimation. First, the IMU pitch angle estimation module estimates the IMU pitch angle using IMU measurements and zero velocity information. Second, the road slope angle estimation module estimates the road slope angle based on the assumption that the vehicle moves in the road slope direction. Finally, the road-to-IMU pitch angle estimation module estimates the road-to-IMU pitch angle using the previously estimated IMU pitch angle and road slope angle.

III. SENSORS AND PRE-PROCESSING

A. COORDINATE SYSTEM

Before introducing the system, the coordinate system and notation are defined. In this system, three main coordinates are defined, as shown in Fig. 5. A navigation frame (n-frame) is a fixed frame that does not move. The z-axis of the n-frame is parallel to gravity, and the x-axis is parallel to the initial heading of the IMU. The road frame (r-frame) is also a fixed frame that does not move. But the z-axis of the r-frame is perpendicular to the road, not perpendicular to gravity. The body frame (b-frame) is an IMU frame in which sensor measurement is measured. Since the IMU is aligned with the headlamp, the b-frame can be regarded as a headlamp frame. Therefore, the IMU frame and headlamp frame are defined as b-frame for convenience. The position, velocity, and acceleration defined in the n-frame are expressed as p^n, v^n, and a^n. In the case of a rotation relationship between two frames, the reference frame is notated in superscript, and the corresponding frame is notated in subscript. For example, the pitch angle of IMU (b-frame) reference to n-frame is notated as θ_b^n.

The expression of orientation can be expressed as Euler angle, direction cosine matrix, and quaternion. Using the traditional z-y-x Euler angles (ψ (yaw), θ (pitch), and ϕ (roll)), the direction cosine matrix (R_b^n) and quaternion (q_b^n) can be expressed as:

$$R_b^n = \begin{bmatrix} c\psi c\theta & c\psi s\theta s\phi - s\psi c\phi & c\psi s\theta c\phi + s\psi s\phi \\ s\psi c\theta & s\psi s\theta s\phi + c\psi c\phi & s\psi s\theta c\phi - c\psi s\phi \\ -s\theta & c\theta s\phi & c\theta c\phi \end{bmatrix} \quad (2)$$

$$q_b^n = \begin{bmatrix} \cos(\psi/2) \\ 0 \\ 0 \\ \sin(\psi/2) \end{bmatrix} \otimes \begin{bmatrix} \cos(\theta/2) \\ 0 \\ \sin(\theta/2) \\ 0 \end{bmatrix} \otimes \begin{bmatrix} \cos(\phi/2) \\ \sin(\phi/2) \\ 0 \\ 0 \end{bmatrix} \quad (3)$$

where 'c' and 's' mean abbreviation of 'cos' and 'sin,' and $\otimes$ is the multiplication of quaternion [26].

B. SENSOR MODELS

The purpose of sensor modelling is to formulate what the sensor measures. In this system, two sensors are modelled. One is the IMU sensor, and the other is the wheel speed sensor.

1) INERTIAL MEASUREMENT UNIT (IMU)

The Inertial Measurement Unit (IMU) consists of two types of sensors: an accelerometer and a gyroscope. Accelerometer measures specific force ($\tilde{f}^b$) and gyroscope measures angular velocity ($\tilde{\omega}^b$). In (4), the specific force includes gravity (g^b) and the acceleration of the IMU (a^b). The error occurring in the accelerometer is defined in two types. One is the bias (δ_a^b), which is a slowly varying value, and the other one is zero mean random noise (e_a^b).

$$\tilde{f}^b = a^b + g^b + \delta_a^b + e_a^b \quad (4)$$

In (5), the gyroscope only measures the angular velocity of the IMU (ω^b). The error occurring in the gyroscope is defined in two types. One is the bias (δ_ω^b) that is slowly varying value and the other one is zero mean random noise (e_ω^b).

$$\tilde{\omega}^b = \omega^b + \delta_\omega^b + e_\omega^b \quad (5)$$

2) WHEEL SPEED SENSOR

Electronic Stability Control (ESC) systems are regulated to be installed in all vehicles. The ESC contains several sensors, among which the wheel speed sensor provides the speed of each wheel of the vehicle. The speed obtained from the wheel speed sensor is used by averaging the speed values of the four wheels as follows:

$$v_{avg} = (v_{rl} + v_{rr} + v_{fl} + v_{fr})/4 \quad (6)$$

where v_{rl}, v_{rr}, v_{fl} and v_{fr} represent the speeds of the left rear wheel, right rear wheel, and left front wheel and right front wheel.

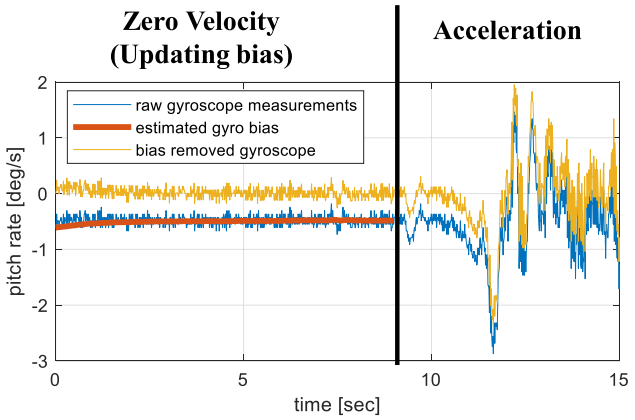

FIGURE 6. At the zero velocity, the bias is estimated using a low-pass filter and the estimated bias is removed. During acceleration, bias-removed gyroscope measurements are output.

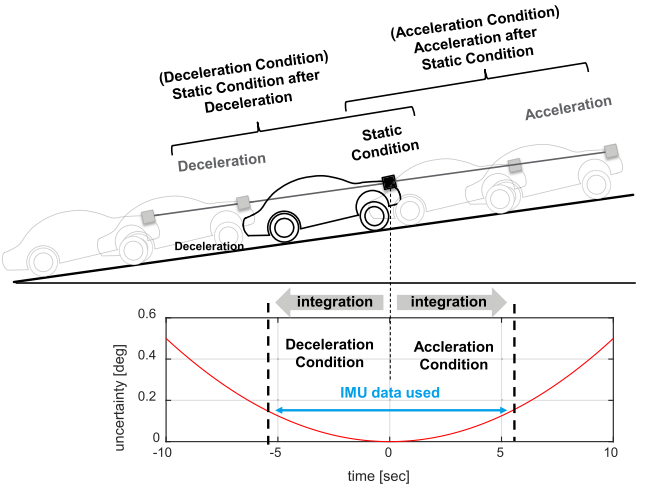

FIGURE 7. There are two operating conditions of the system: deceleration condition and acceleration condition. Static condition after deceleration and acceleration after the static condition is defined before and after the static condition, respectively. Only short-term IMU data with low uncertainty are used. The reason for setting the condition in this way is to use states with low uncertainty near static conditions.

C. PRE-PROCESSING

1) ZERO VELOCITY DETECTION

The purpose of the zero velocity detection module is to detect the stationary state of the IMU. The wheel speed sensor is used to detect zero velocity. Since the wheel speed sensor directly measures the speed of the vehicle, zero output from the wheel speed sensor means the stationary state of the IMU. The catastrophe that can occur with a wheel speed sensor is when it is perceived as stationary while moving. So the algorithm for detecting zero velocity works conservatively. The zero velocity is only detected if the wheel speed sensor data outputs zero for a certain amount of time back and forth.

2) CALIBRATION

The purpose of the calibration module is to remove the bias of the gyroscope (δ_ω^b). The gyroscope error consists of bias and high-frequency noise, as shown in (5). If the bias is not removed, the bias is integrated when the angular velocity is integrated, resulting in drift error. Therefore, a slowly varying bias of the gyroscope (δ_ω^b) is estimated and removed in this module.

Calibration operates in two ways based on the stop information obtained from the zero velocity detection module. First, when zero velocity is recognized, angular velocity (ω_b) should output zero. However, measurements in zero velocity include bias (δ_ω^b) and high-frequency noise (e_ω^b). By reflecting the characteristics of the two errors, bias is estimated using a first-order recursive low-pass filter (7). A low-pass filter removes high-frequency values from high-frequency noise and passes only low-frequency values. As shown in Fig. 6, high-frequency noise is removed in the zero velocity state, showing that the bias is estimated.

$$\hat{\delta}_{\omega,t} = \alpha * \tilde{\omega}_t^b + (1-\alpha) * \hat{\delta}_{\omega,t-1} \tag{7}$$

α is the coefficient of the first-order low-pass filter and determines the cutoff frequency. The larger the α, the more the latest measured value is weighted. Second, gyroscope bias is removed using an estimated bias in (7). The bias removed gyroscope output ($\hat{\omega}_t^b$) is obtained using (8). As shown in Fig. 6, bias-removed gyroscope measurement is output during acceleration.

$$\hat{\omega}_t^b = \tilde{\omega}_t^b - \hat{\delta}_{\omega,t} \tag{8}$$

IV. ROAD TO HEADLAMP PITCH ANGLE ESTIMATION

In the road-to-headlamp pitch angle estimation part, IMU pitch angle, road slope angle, and road-to-IMU pitch angle are estimated in order as shown in Fig. 4 (b). First, the IMU pitch angle estimation module estimates the IMU pitch angle through the switching method using static information. Second, the road slope angle estimation module estimates the road slope angle under the assumption that the vehicle moves along the road slope. Finally, the road-to-IMU pitch angle estimation estimates the road-to-IMU pitch angle using the angles estimated from the previous two modules.

The proposed system estimates the road-to-IMU pitch angle when one of the operation conditions is met. As shown in Fig. 7, two kinds of operating conditions exist. The first is static conditions after deceleration, and the second is acceleration after static conditions. The static condition information is obtained from the zero velocity module (III-C1), and the operating conditions can be detected. The reason for including the static condition in the operating condition is twofold. First, as shown in Fig. 7, the state uncertainty is the lowest in the static condition. Only short-term IMU data with low uncertainty can be used. Second, drift errors can be minimized by using the latest updated bias. When the static condition is detected, the states like attitude (roll and pitch) and velocity can be estimated. Attitude is estimated using gravity from the accelerometer when velocity is estimated as zero. In the case of static conditions after the deceleration, integration is performed from the static states in reverse

order of time. Since the proposed system operates in quasi-real time, in deceleration conditions, the deceleration IMU data can be saved, and then inverse time integration can be performed.

A. IMU PITCH ANGLE ESTIMATION

The purpose of IMU pitch angle estimation is to estimate the orientation (roll, pitch, and yaw) of the IMU, including the IMU pitch angle (θ_b^n) as shown in Fig. 3. Two methods are used to estimate orientation using IMU. First, the attitude is estimated using the gravity measured by the accelerometer. It can be used in a stationary state without external acceleration. Second, the orientation is estimated by integrating the gyroscope. It can be estimated when moving with external acceleration. However, drift error occurs by integrating the bias. In this paper, the switching method is used, which estimates the attitude(roll and pitch) using an accelerometer when static conditions and a gyroscope when dynamic conditions. The stop information is obtained from the zero velocity module (III-C1).

In the static condition, the attitude (roll and pitch) is estimated as follows:

$$\hat{\phi}_b^n = \tan^{-1}\left(\frac{g_y^b}{g_z^b}\right)$$
$$\hat{\theta}_b^n = \tan^{-1}\left(\frac{-g_x^b}{g_y^b/\sin\hat{\phi}^n}\right) \tag{9}$$

where the gravity (g_x^b, g_y^b, g_z^b) is the average value measured from the accelerometer in a static condition [27].

In the dynamic condition, the orientation is estimated by integrating the angular velocity from the gyroscope. In (10), a quaternion-based prediction model is used [28]. This method uses bias-removed angular velocity ($\hat{\omega}_t$) as input and estimates the state of the next time step from the state of the previous time step. In the case of the deceleration condition, the time difference (Δt) is set to negative. The attitude (roll and pitch) obtained using (9) is used as an initial value, and yaw is initialized to zero. The initial attitude presented in the Euler angle is converted into quaternion using (3).

$$q_{b,t+1}^n = [\cos(\Theta/2)I + \frac{\sin(\Theta)/2}{\Theta/2} \cdot A \cdot dt]q_{b,t}^n \tag{10}$$

A, and Θ are composed as follows.

$$A = \frac{1}{2}\begin{bmatrix} 0 & -\omega_x & -\omega_y & -\omega_z \\ \omega_x & 0 & \omega_z & -\omega_y \\ \omega_y & -\omega_z & 0 & \omega_x \\ \omega_z & \omega_y & -\omega_x & 0 \end{bmatrix}$$
$$\Theta = \sqrt{(\omega_x)^2 + (\omega_y)^2 + (\omega_z)^2} \cdot \Delta t \tag{11}$$

Finally, the estimated pitch using (9) is used as the IMU pitch angle ($\hat{\theta}_b^n$) in Fig. 3.

B. ROAD SLOPE ANGLE ESTIMATION

The purpose of road slope estimation is to estimate road slope angle based on the assumption that the vehicle must move along the road. As shown in Fig. 8, the IMU moves in the same direction as the road regardless of the load on the vehicle. Therefore, position-based road slope estimation is performed. The position-based road slope angle estimation is a method of using the trajectory of the IMU. Based on the assumption that the trajectory of the IMU is parallel to the road slope angle, the road slope angle can be estimated. As shown in Fig. 9, the proposed system consists of the IMU-based dead reckoning step that estimates the position and the road slope estimation step that estimates the road slope angle using the assumption.

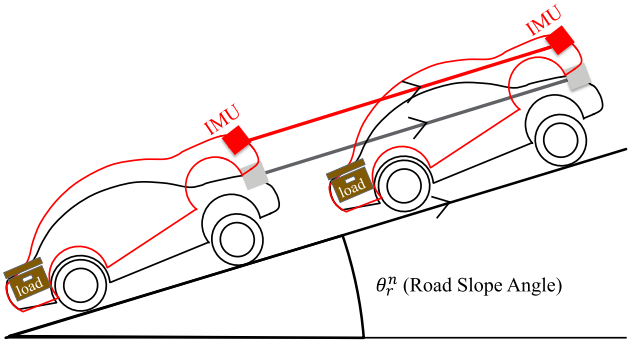

FIGURE 8. The trajectory of the IMU is parallel to the road slope regardless of vehicle lift due to load. At a constant road slope, the following assumptions are possible and are applied for short distances.

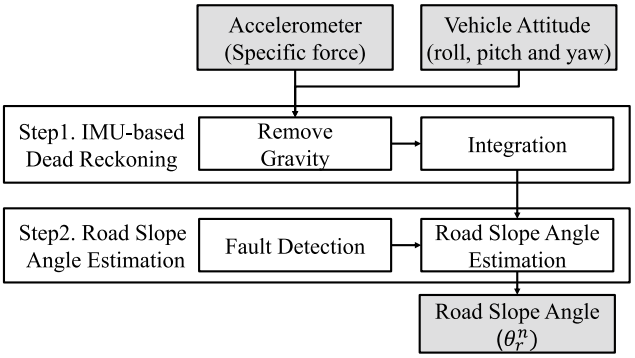

FIGURE 9. The road slope estimation module architecture consists of two steps. In the first step, the position is estimated by performing a dead reckoning based on the IMU value [25]. In the second step, the road slope is estimated, and the case where the road slope changes are removed.

The first step, IMU-based dead reckoning, is to estimate the position (p^n) of the IMU [25]. In (12), the Constant Acceleration (CA) prediction model is used to estimate the position of the IMU. The accelerometer measurement and the orientation obtained from the IMU pitch estimation module (IV-A) are used as input. The specific force from the accelerometer includes both gravity and the acceleration of the IMU. If gravity is not removed, gravity is integrated, and a drift error occurs in the position estimation. Therefore, (12) includes the process of removing gravity (g^n) from the measured specific force ($\tilde{f}_t^b$).

The specific force ($\tilde{f}_t^b$) measured in the b-frame must be converted into the n-frame to remove gravity. Since the z-axis

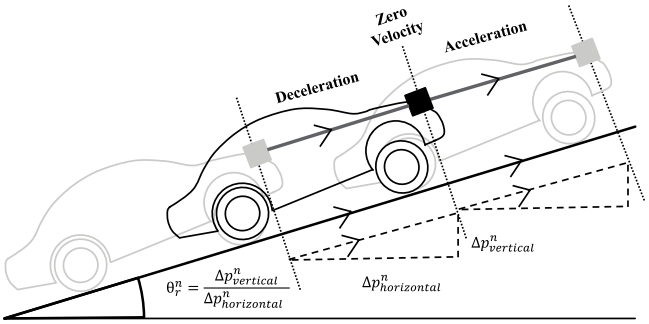

FIGURE 10. Assuming that the road slope is constant over short distances, the equation is derived. The road slope is defined as the ratio of horizontal displacement to vertical displacement.

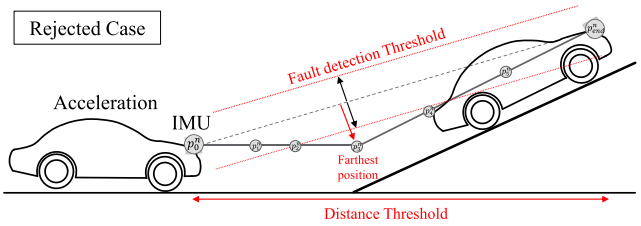

FIGURE 11. IMU data from the non-constant road is rejected. When the farthest position of the IMU is out of a certain threshold, it is determined that the road slope changes.

of the n-frame is the gravity direction, so gravity consists only of the z component ($g^n = [0, 0, g^n_z]$). By using the orientation (R^n_b) obtained from IV-A, the specific force can be converted to an n-frame, and gravity can be removed. The acceleration without gravity is integrated using a constant acceleration model. In the case of the deceleration condition, delta time (Δt) is set as a minus.

$$p^n_{t+1} = p^n_t + \Delta t \cdot v^n_t + \frac{\Delta t^2}{2} \cdot (R^n_{b,t}\tilde{f}^b_t - g^n) \tag{12}$$

In the above equation, the velocity of the IMU (v^n_t) is obtained by (13). The rotation matrix from n-frame to b-frame ($R^n_{b,t}$) is obtained by transforming the quaternion output ($q^n_{b,t}$) of IMU pitch angle estimation module (IV-A) using (3).

$$v^n_{t+1} = v^n_t + \Delta t \cdot (R^n_{b,t}\tilde{f}^b_t - g^n) \tag{13}$$

The second step, road slope estimation, is to estimate road slope angle (θ^n_r) using positions of the IMU (p^n_x, p^n_y, and p^n_z). As shown in Fig. 8, the road slope estimation model has based on the assumption that the vehicle moves parallel to the road slope regardless of the vehicle pitch changes due to the loading conditions. As shown in Fig. 10, the vertical positions ($\Delta p^n_{vertical}$) and horizontal position ($\Delta p^n_{z,horizontal}$) are separated to estimate the road slope. Road slope angle is estimated as the ratio of the horizontal position and vertical position difference as follows:

$$\hat{\theta^n_r} = \arctan(\frac{\Delta p^n_{vertical}}{\Delta p^n_{horizon}}) \tag{14}$$

where $\Delta p_{vertical}$, $\Delta p_{horizon}$ is vertical and horizontal position difference shown in (15). T_d is a value determined by the horizontal movement distance threshold of the IMU, which is adjustable. T_d is set to a value small enough to consider that the slope of the road is constant as shown in Fig. 10.

$$\begin{aligned} \Delta p^n_{vertical} &= p^n_{z,T_d} - p^n_{z,0} \\ \Delta p^n_{horizon} &= \sum_{t=1}^{t=T_d} \sqrt{(p^n_{x,t} - p^n_{x,t-1})^2 + (p^n_{y,t} - p^n_{y,t-1})^2} \end{aligned} \tag{15}$$

Fault detection in the second step rejects data whose road slope is not constant. As shown in Fig. 8, (15) estimates the road slope angle based on the assumption that the road slope is constant. In cases where the road slope changes, such as Fig. 11, (15) cannot be used. To reject cases where the assumptions do not meet, the position of the IMU (p^n_0, p^n_1, $p^n_2 \ldots, p^n_{end}$) obtained from the IMU-based dead-reckoning step is used [25]. If the line is drawn at both ends of the road slope to be estimated and the value farthest from the line among the position of the IMU exceeds a certain threshold, the road slope is not estimated and is rejected.

C. ROAD TO VEHICLE PITCH ESTIMATION

Using the IMU pitch angle from (9) and the road slope angle from (14), the road-to-IMU pitch angle is estimated easily using (16). As mentioned in Fig. 7, when the operating condition is met, the road-to-IMU pitch angle is estimated once. The estimated road-to-IMU pitch angles are numbered $\tilde{\theta}^r_{b,1}, \tilde{\theta}^r_{b,2}, \tilde{\theta}^r_{b,3} \ldots \tilde{\theta}^r_{b,t}$.

$$\tilde{\theta}^r_{b,t} = \hat{\theta}^n_{b,t} - \hat{\theta}^n_{r,t} \tag{16}$$

The obtained road-to-IMU pitch angle is averaged using (17). The purpose of averaging is to compensate for performance degradation caused by random walk during integration. Because the more road-to-IMU pitch angles averaged, the more reliable the estimate is.

$$\hat{\theta}^r_{b,t} = \frac{(m-1)\hat{\theta}^r_{b,t-1} + \tilde{\theta}^r_{b,t}}{m} \tag{17}$$

m represents the number of estimated road-to-IMU pitch angles.

V. VERIFICATION

The verification consists of three parts: simulation, test road experiment, and common road experiment. First, in the simulation, the effect of the IMU sensor noise is analyzed. Second, in the test road experiment, an IMU is attached to the vehicle, and the performance of the proposed system is evaluated. Third, in the common road experiment, the robustness of this system is verified in a general urban driving environment.

A. SIMULATION

The purpose of the simulation is to analyze the effects of the accelerometer bias (δ^b_a) and accelerometer high-frequency noise (e^b_a) in (4). Gyroscope bias and gyroscope high-frequency noise are not considered because the bias of

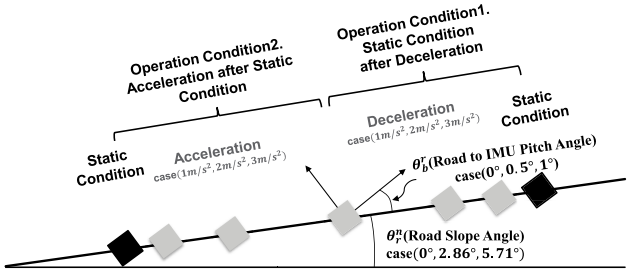

FIGURE 12. In the simulation, generated motion is in the order of stop-acceleration-deceleration-stop at a constant road slope. At this time, two system operating conditions are satisfied. There are three control variables that can be adjusted: the road slope angle, the road-to-IMU pitch angle, and the magnitude of the acceleration.

TABLE 1. Simulation control variables.

Control Variables	Values
Road Slope Angle	$0\%, 5\%, 10\%\ (= 0°, 2.86°, 5.71°)$
Road-to-IMU Pitch Angle	$0°, 0.5°, 1°$
Magnitude of Acceleration	$1m/s^2, 2m/s^2, 3m/s^2$

the gyroscope is removed in pre-processing, and the high-frequency noise of the gyroscope has little effect. Therefore, simulation consists of two parts: accelerometer bias simulation and accelerometer high-frequency noise simulation. First, in the accelerometer bias simulation, the estimation error of the proposed system is analyzed while increasing the accelerometer bias as an independent variable. Second, in the accelerometer high-frequency noise simulation, the estimation error of the proposed system is also analyzed by changing the accelerometer noise density. There are three control variables in both simulations, as shown in Table. 1: road slope angle, road-to-IMU pitch angle, and magnitude of the acceleration.

The simulation motion data is configured to perform linear motion as shown in Fig. 12. The reason for the linear motion is to exclude the effect of vehicles (vehicle vibration and pitch motion) and non-uniform road slope angle. The motion is in the order of stop-acceleration-deceleration-stop. Since two system operating conditions are satisfied in one motion, two estimations are performed. For sensor simulation, the ''imuSensor'' function of the MATLAB navigation toolbox was used. high-frequency noise and bias were generated by setting the noise density and constant bias of the IMU. high-frequency noise is Gaussian noise determined by noise density and sampling frequency, and bias is constant bias.

1) ACCELEROMETER BIAS SIMULATION

The purpose of accelerometer bias simulation is to evaluate the effect of bias on the performance of the proposed estimation system. The analysis is divided into three parts according to the three types of control variables: road slope angle, road-to-IMU pitch angle, and the magnitude of acceleration. Control variables are set as shown in the Table. 1. The road slope was set to 0%, 5%, and 10%, which is a typical urban road slope angle. The road-to-IMU pitch angle was set to 0°, 0.5°,

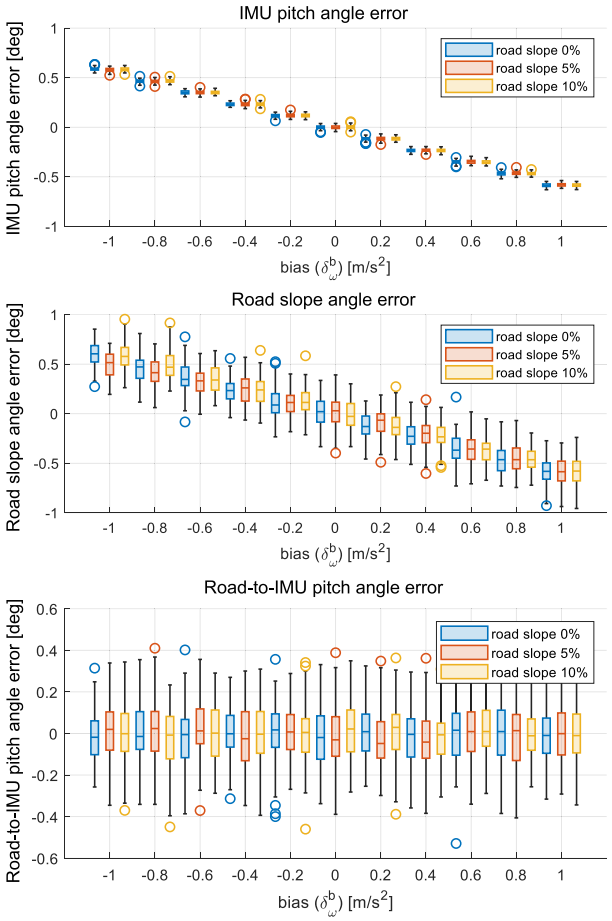

FIGURE 13. The estimation performance is evaluated by changing the road slope to 0%, 5%, and 10% among the control variables. Each estimation error is shown as the bias increases. From the top, it is the estimation error of IMU pitch angle, road slope angle, and road-to-IMU pitch angle, respectively.

and 1°. The reason why the interval was set to 0.5° is because of the range angle of UNECE regulations. The magnitude of the acceleration was set to $1m/s^2$, $2m/s^2$, and $3m/s^2$, which is the range that includes normal acceleration and sudden acceleration. The independent variable, accelerometer bias, is changed from $-1m/s^2$ to $1m/s^2$ at an interval of $0.2m/s^2$. To evaluate the effect of high-frequency noise as well, the accelerometer noise density is set to $300\mu g/\sqrt{Hz}$, according to low-cost IMU specifications. For each bias setting, 50 movements are performed, and the total operating conditions are satisfied 100 times.

First, the effect of the accelerometer bias is analyzed by changing the road slope angle variable to 0°, 2.86°, and 5.71°. Another control variable, road-to-IMU pitch angle, is set to 0° and the magnitude of the acceleration is set to $2m/s^2$. The estimation errors of IMU pitch angle, road slope angle, and road-to-IMU pitch angle are analyzed in Fig. 13. There is no change in the estimation error as the road slope increases. The accelerometer bias causes an error when estimating the IMU pitch angle in (9). As the magnitude of the bias increases, the IMU pitch angle estimation error also increases. Since IMU

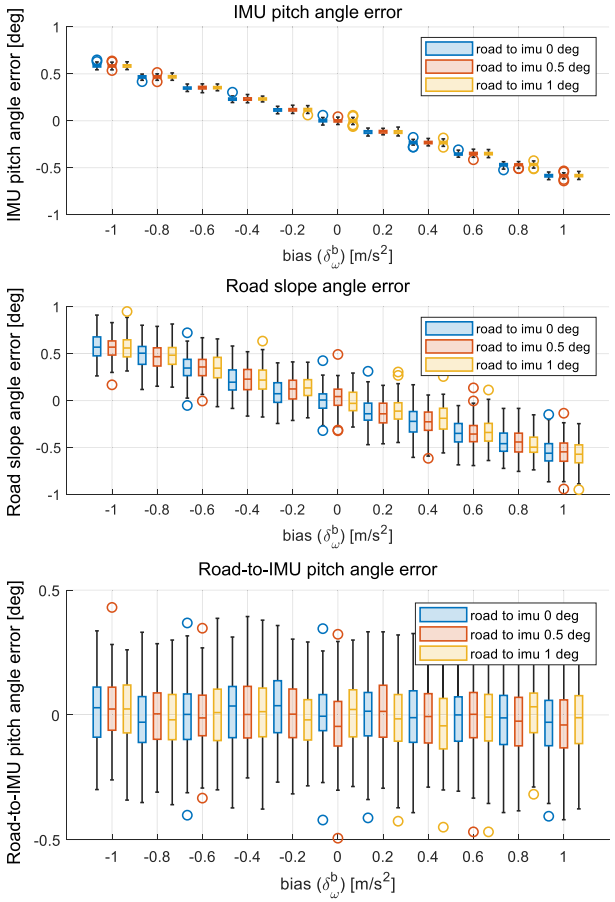

FIGURE 14. The control variable road-to-IMU pitch angle is changed to 0°, 0.5°, and 1°. Estimation errors of IMU pitch angle, road slope angle, and road-to-IMU pitch angle according to the increase in accelerometer bias are shown in order from the top.

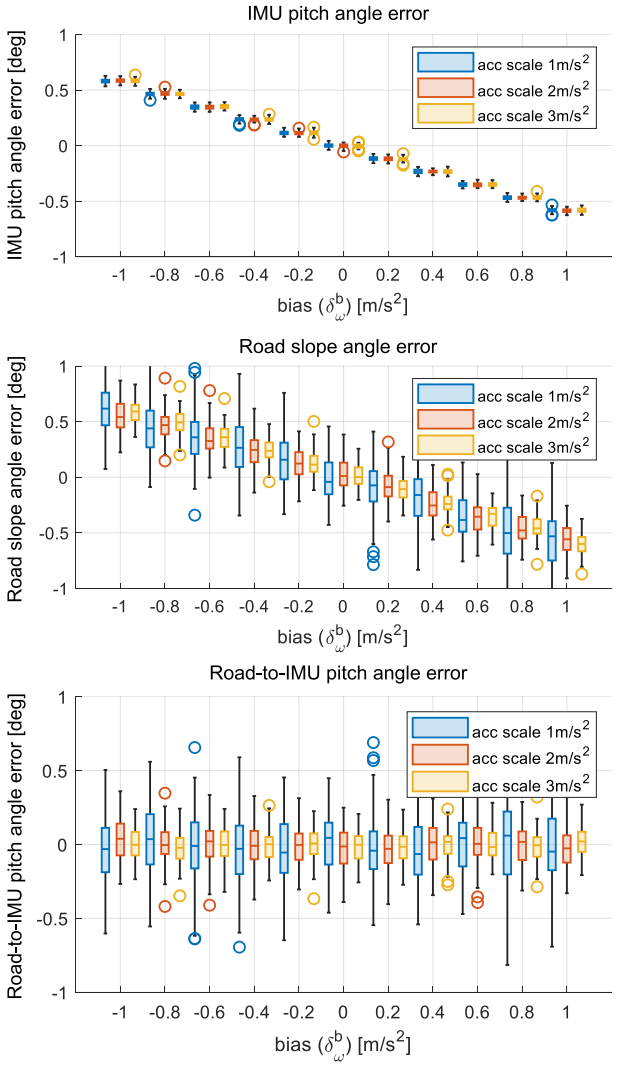

FIGURE 15. The magnitude of the acceleration is changed to $1m/s^2$, $2m/s^2$, and $3m/s^2$. Estimation errors of IMU pitch angle, road slope angle, and road-to-IMU pitch angle are indicated from the top.

pitch angle is used as the initial value in (10), the same error occurs in the road slope angle estimation. However, since the road slope angle is subtracted from the IMU pitch angle in (16), the error caused by the bias is cancelled out. Finally, the road-to-IMU pitch angle estimation error required for headlamp leveling shows an error of a zero mean.

Second, the effect of the accelerometer bias is analyzed by changing the control variable, road-to-IMU pitch angle, to 0°, 0.5°, and 1°. Another control variable, road slope angle, is set to 0°, and the magnitude of the acceleration is set to $2m/s^2$. The estimation errors of IMU pitch angle, road slope angle, and road-to-IMU pitch angle are sequentially shown in Fig. 14. The result is the same as the previous simulation. The increase in accelerometer bias affects the IMU pitch angle estimation error and the road slope angle estimation error. However, the road-to-IMU pitch angle estimation error is not affected and is a zero mean. Finally, the road-to-IMU pitch angle estimation error is not affected by the change in the road-to-IMU pitch angle, which is a control variable.

Third, the scale of acceleration is changed to $1m/s^2$, $2m/s^2$, and $3m/s^2$. Another control variable, road slope angle, is set to 0°, and road-to-IMU pitch angle is set to 0°. The estimation errors of IMU pitch angle, road slope angle, and road-to-IMU pitch angle are shown in Fig. 15. As the accelerometer bias increases, the IMU pitch angle estimation error and the road slope angle estimation error increase. However, road-to-IMU pitch angle estimation error is not affected by the accelerometer bias. Unlike the previous control variables, road slope and road-to-IMU pitch angle, the magnitude of the acceleration reduces the variance of the road slope angle estimation error. In (15), T_d is determined according to the set distance and is set to 2 meters in this simulation. When the acceleration is large, the time to reach 2 meters is shortened, the number of samples to be integrated decreases, and the random walk by high-frequency noise integration decreases.

2) ACCELEROMETER HIGH-FREQUENCY NOISE SIMULATION

The purpose of this part is to analyze the effect of accelerometer high-frequency noise on the proposed system. Since

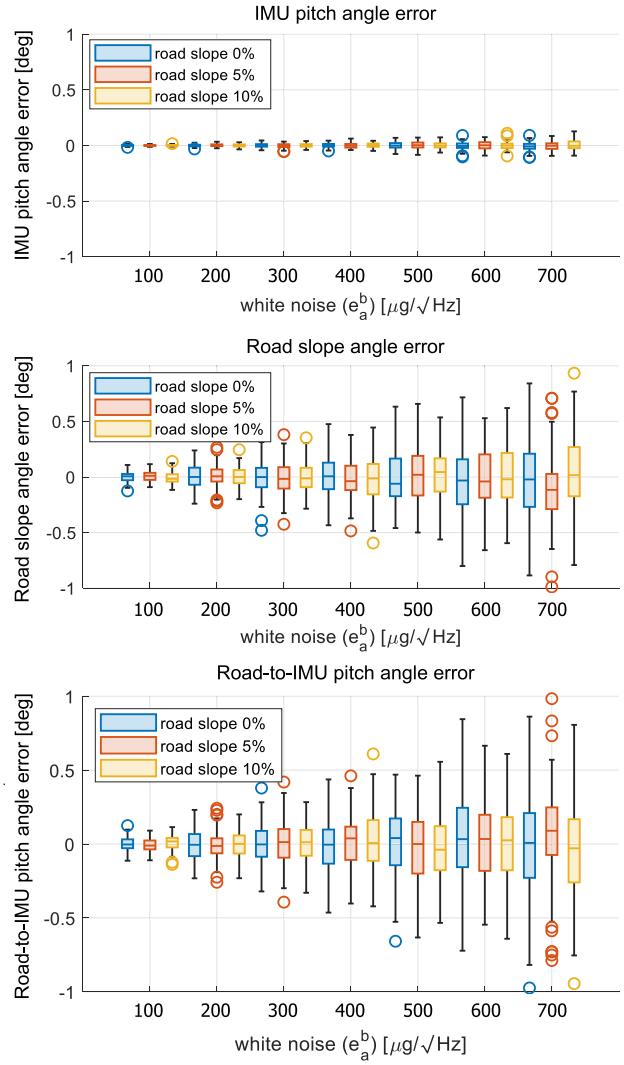

FIGURE 16. The road slope, which is a control variable, changes to 0°, 5°, and 10°, indicating an estimation error. It shows the estimation error as the high-frequency noise increases. From the top, the estimation error of IMU pitch angle, road slope angle, and road-to-IMU pitch angle are shown, respectively.

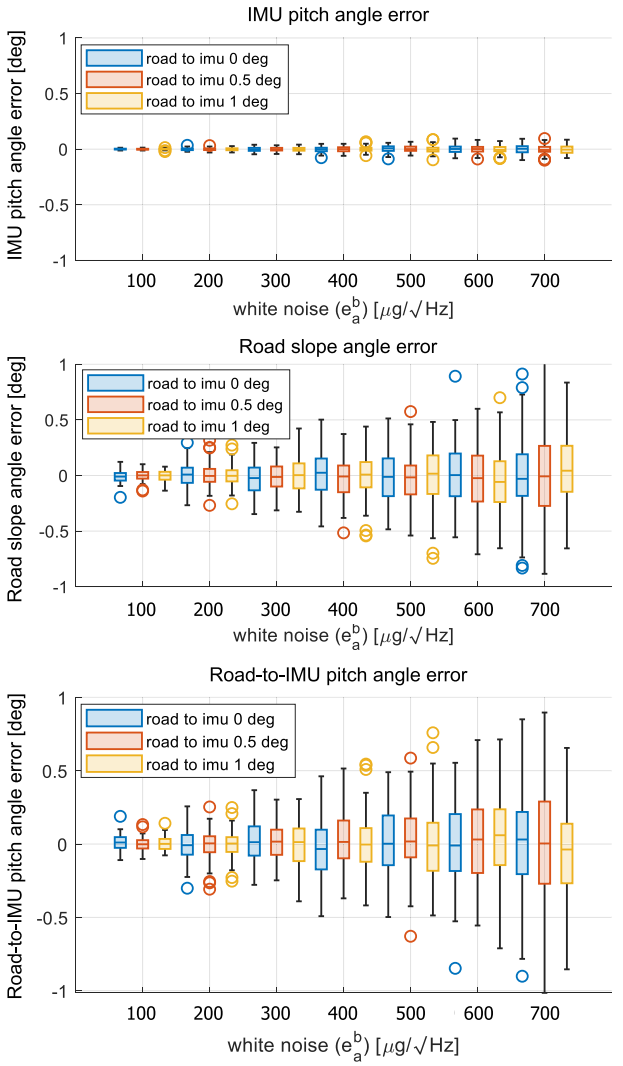

FIGURE 17. The road-to-IMU pitch angle, which is a control variable, is changed to 0°, 0.5°, and 1°. The performance of IMU pitch angle estimation module, road slope angle estimation module, and road-to-IMU pitch angle estimation module are evaluated according to the increase in noise density. The performance of the angle estimation module. From the top, the estimation errors of IMU pitch angle, road slope angle, and road-to-IMU pitch angle are shown.

high-frequency noise randomly generates different noises, 50 simulations were performed for each control variable to verify the performance of the proposed system, and the road-to-IMU pitch angle was estimated 100 times. The effect of estimation error is evaluated by changing the noise density from $100\mu g/\sqrt{Hz}$ to $700\mu g/\sqrt{Hz}$, which is the high-frequency noise performance of the IMU.

First, the estimation errors of the proposed system are evaluated by changing the road slope angle to 0°, 2.86°, and 5.71°. The estimation error of IMU pitch angle, road slope angle, and road-to-IMU pitch angle according to the increase in accelerometer noise density are shown in Fig. 16. The road slope angle has no effect on the estimation error. The accelerometer high-frequency noise has little effect on IMU pitch angle estimation less than 0.1°, but it has a large effect on road slope angle estimation. As the noise density increases, the variance of the road slope estimation error increases up to 1°, and the average also fluctuates. Because when integrating the accelerometer in (11), high-frequency noise is also integrated, causing a random walk. As a result, high-frequency noise increases the variance of the road-to-IMU pitch angle estimation error and the road slope angle does not affect the estimation errors.

Second, the road-to-IMU pitch angle is changed to 0°, 0.5°, and 1°. The estimation error of the proposed system is evaluated. Other control variables, road slope angle and magnitude of acceleration are set to 0° and $2m/s^2$, respectively. The estimation errors of IMU pitch angle, road slope angle, and road-to-IMU pitch angle are shown in Fig. 17. The road-to-IMU pitch angle has no effect on the estimation performance of the proposed system. As in the previous experimental

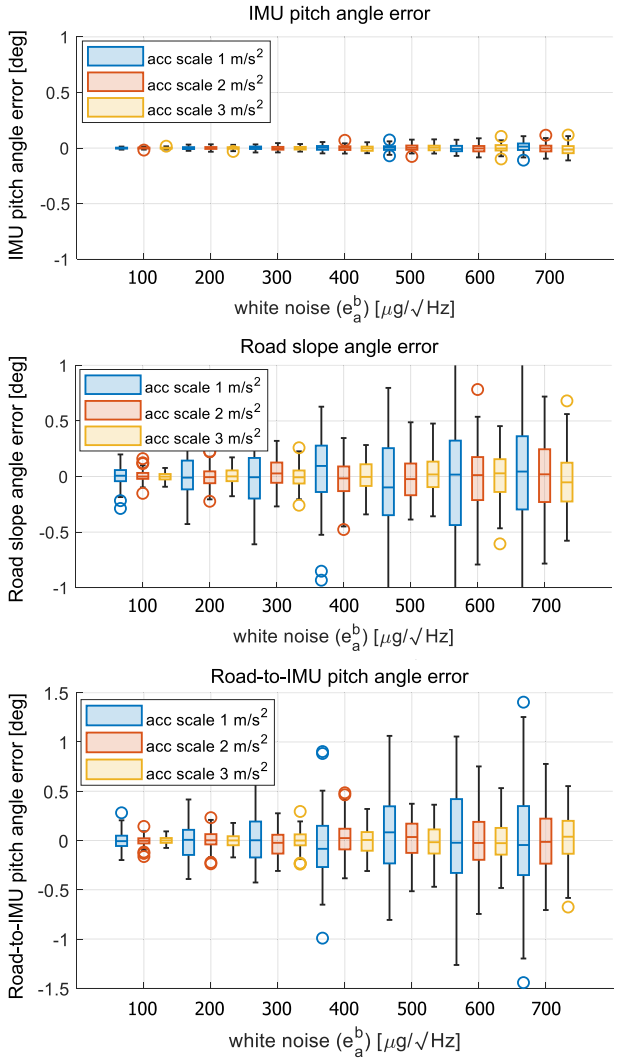

FIGURE 18. The magnitude of the acceleration changes as $1m/s^2$, $2m/s^2$, and $3m/s^2$. As high-frequency noise increases, estimation errors of the IMU pitch angle estimation module, road slope angle estimation module, and road-to-IMU pitch angle estimation module are analyzed.

results, the accelerometer noise density increases the estimation variance of road slope angle estimation and road-to-IMU pitch angle.

Third, the magnitude of the acceleration is changed to $1m/s^2$, $2m/s^2$, and $3m/s^2$. Other control variables, road slope angle and road-to-IMU pitch angle are both set to 0°. Fig. 18 shows the estimation errors of IMU pitch angle, road slope angle, and road-to-IMU pitch angle. As in the previous experiment, the estimated variance of road slope angle estimation and road-to-IMU pitch angle estimation increases as the accelerometer noise density increases. However, in the road slope angle estimation, the magnitude of the acceleration reduces the estimation variance of road slope angle and road-to-IMU pitch angle. In (15), T_d is determined according to the distance. If the acceleration is large, the time to reach 2 meters becomes shorter and the number of samples to be

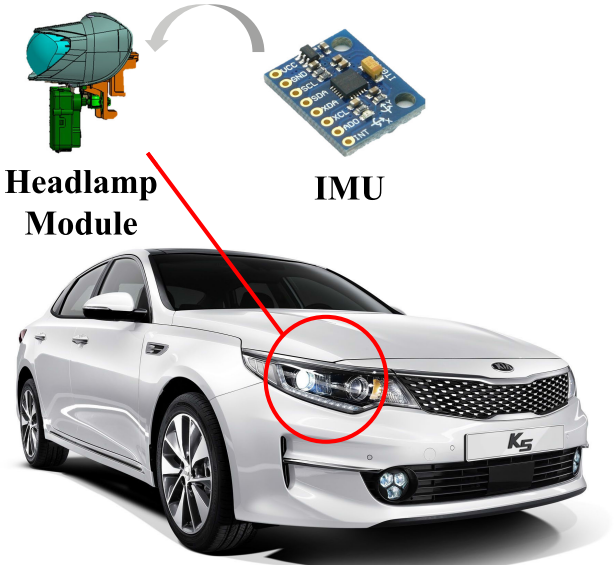

FIGURE 19. The test vehicle is the vehicle model K5. The experiment was carried out by installing the IMU at the position of the headlamp Electric Controller Unit (ECU). The low-cost IMU is a model "mpu-6050," and the noise density has a performance of $300\mu g/\sqrt{Hz}$.

integrated decreases. That is, as the acceleration increases, the random walk by integration decreases, and the road slope angle estimation variance decrease.

In summary, accelerometer bias affects the IMU pitch angle estimation and road slope angle estimation but does not affect the road-to-IMU pitch angle estimation. Accelerometer high-frequency noise affects the variance of road slope angle estimation and road-to-IMU pitch angle estimation. The control variables, road slope angle and road-to-IMU pitch angle do not affect the estimation performance. However, as the magnitude of the acceleration increases, the variance of road slope angle estimation and road-to-IMU pitch angle estimation becomes smaller.

B. TEST ROAD EXPERIMENTS

The purpose of the test road experiment is to evaluate the performance of the proposed system in the vehicle. As shown in Fig. 19, the vehicle environment was configured by attaching the IMU to the headlamp of the vehicle model K5. The IMU model is mpu-6050, which consists of a 3-axis accelerometer and a 3-axis gyroscope. The output frequency is 100Hz. The detailed specifications of the IMU are as follows. The noise densities of the accelerometer and gyroscope are $300\mu g/\sqrt{Hz}$ and $0.01°/\sqrt{Hz}$, respectively. The bias changes due to the change in temperature of the accelerometer and gyroscope are $0.032\%/°C$ and $0.026\%/°C$, respectively.

The ground truth of the road-to-IMU pitch angle is measured using (9) on the surface where the road slope angle is zero. When (9) is used, as in the result of accelerometer bias simulation (V-A1), bias causes an error in IMU pitch angle estimation. The IMU accelerometer bias is removed through the multi-position calibration method [29], and the

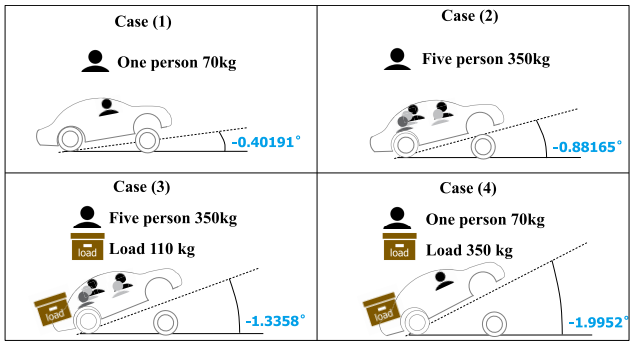

FIGURE 20. The load conditions consisted of four. From the minimum load condition to the maximum load condition, the 1.6° road-to-IMU pitch angle change was measured. The road-to-IMU pitch angle is measured on a surface with zero road slope angle.

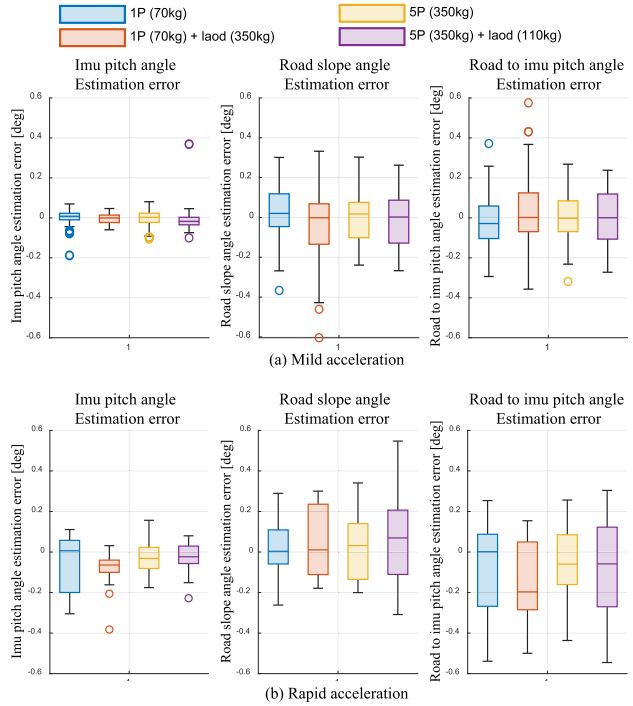

FIGURE 21. For load condition cases (1) to (4), mild acceleration and rapid acceleration were tested. In (a), the experiment was conducted with mild acceleration, and in (b), the experiment was conducted with rapid acceleration.

bias-removed accelerometer accurately measures the road-to-IMU pitch angle. On the road at 0 deg, the IMU and headlamps can also be aligned. As shown in Fig. 20, The road-to-IMU pitch angle was measured according to four load conditions. From case (1) to case (4), a maximum of 1.6° vehicle lift occurs.

The first experiment is divided into mild acceleration and rapid acceleration. In order to evaluate the effect of high-frequency noise, 60 estimations were made for each case. The experimental results with mild acceleration are shown in Fig. 21 (a), and the results with rapid acceleration are shown in Fig. 21 (b). In the case of mild acceleration, the errors and variances of IMU pitch angle, road slope angle, and

FIGURE 22. The test road has three road grades: 0%, 5%, and 15% and has a constant road grade.

road-to-IMU pitch angle are the same as accelerometer bias simulation results (V-A). The estimated variance of the IMU pitch angle is smaller than the estimated variance of the road slope angle, and there is no effect by bias. However, contrary to the result of Fig. 18, when the experiment was performed with a large rapid acceleration, the variance of the road slope estimation increased compared to the experiment with a mild acceleration. This is because, during rapid acceleration, linear motion cannot be achieved due to the pitch motion of the vehicle. Even in the rapid acceleration, the mean error of road-to-IMU pitch angle estimation performance is within 0.2° that can satisfy regulation.

The second experiment evaluates the road-to-IMU pitch angle estimation performance at various road slopes. As shown in Fig. 22, There is a test road with constant road slope angles of 0%, 5%, and 15%. The road slope is divided into uphill and downhill and consists of five road slope cases: 0%, uphill 5%, uphill 15%, downhill 5%, and downhill 15%. In order to evaluate the high-frequency noise of the IMU, 60 estimations were made for each case. In addition, two load conditions were tested to check whether the vehicle lift was recognizable.

The experimental results are divided into two parts. One is shown in Fig. 23 (a) when one person is riding, and another one is shown in Fig. 23 (b) when one person and a load of 350kg is loaded. Based on the simulation result of Fig. 13, the mean errors of the IMU pitch angle and road slope angle can occur by the bias of the accelerometer. However, the road-to-IMU pitch angle estimation error is not due to accelerometer bias. This is because, on the ramp, the force of the front and rear suspension of the axle is different, and the road-to-IMU pitch angle is changed. The error of the road-to-IMU pitch angle is the largest at 0.2° at 15%, but it satisfies the regulation.

C. COMMON ROAD EXPERIMENTS

This experiment verifies the precision and accuracy of the proposed algorithm in the common road. There are two comparison algorithms that propose a road-to-headlamp pitch angle estimation system using an IMU sensor [8], [9]. As shown in Fig. 24, the experiment was conducted in the city of Seoul. The vehicle travelled 8.5 km in 20 minutes at an average speed of about $50km/h$. Experimental data is shown in Fig. 25, which shows accelerometer data and wheel

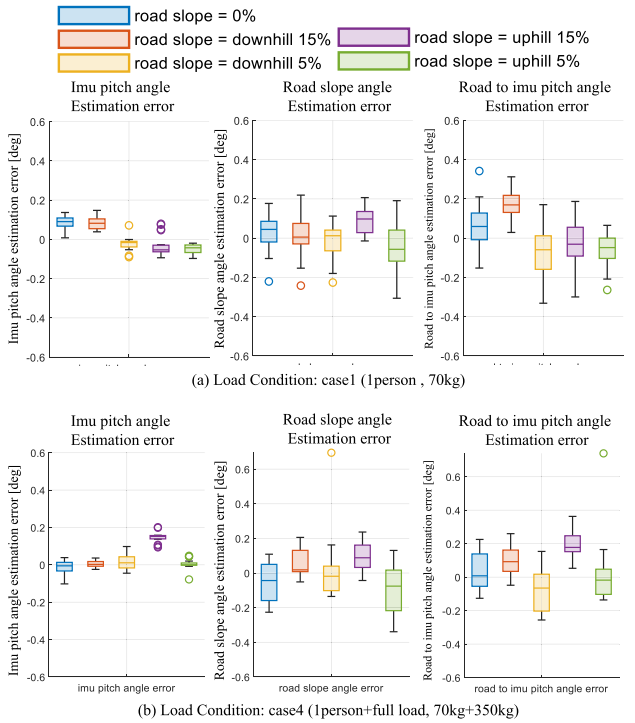

FIGURE 23. The load conditions were tested with the case (1) load condition in (a) and the case (4) load condition in (b). The experimental diversity of the road slope is 0%, uphill 5%, downhill 5%, uphill 15%, downhill 15%.

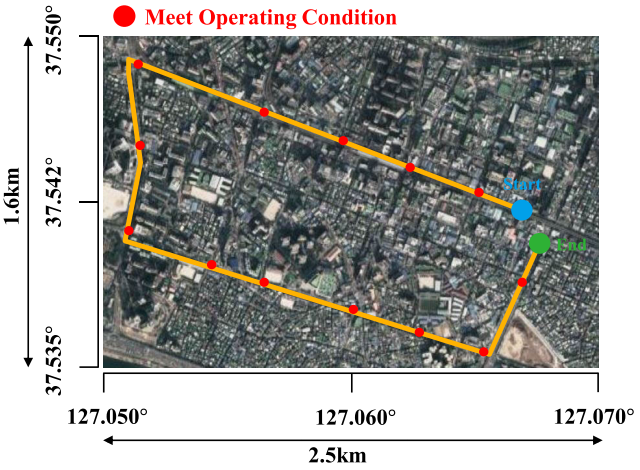

FIGURE 24. The experiment was conducted in the city of Seoul, and a distance of about 8.5km was driven. The vehicle was stopped due to traffic signals and traffic jams, and the operating conditions of the system were satisfied 20 times.

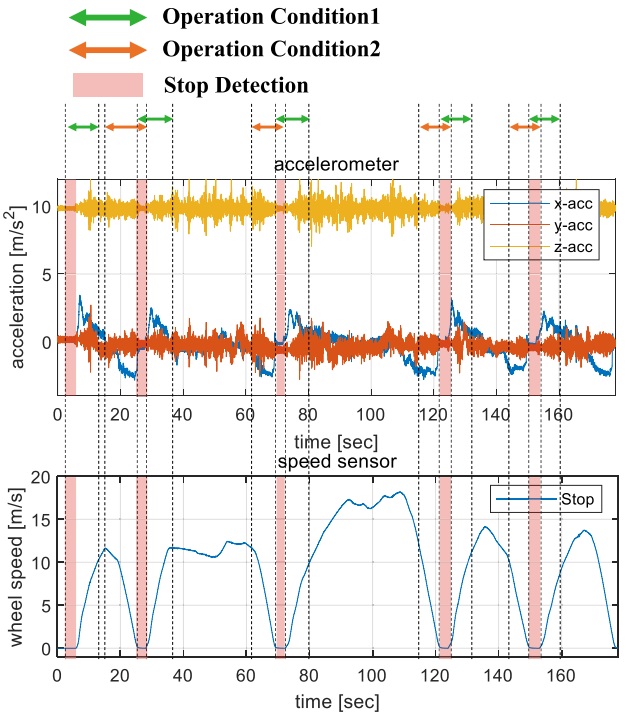

FIGURE 25. Acquired IMU accelerometer data and wheel speed sensor data are shown. Using the wheel speed sensor's stop information, the operating condition of the proposed system is satisfied. 28 operating conditions were satisfied in the acquired data.

TABLE 2. The mean error of common road experiments.

Methods	Mean Error	
	1P (70kg)	5P (350kg)
Ours	0.04°	0.11°
Kasaba [9]	0.38°	0.19°
Nilson [8]	0.53°	1.1°

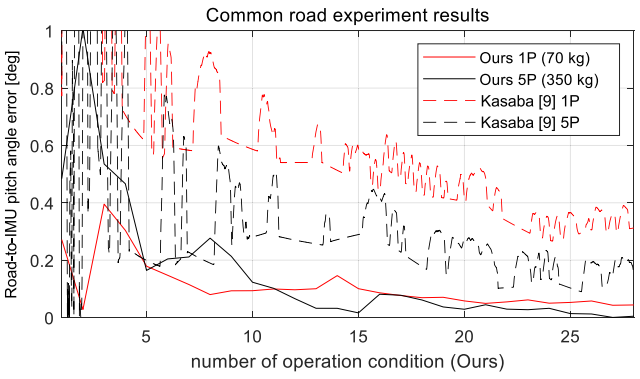

FIGURE 26. It shows the updated road-to-IMU pitch angle estimation error results whenever the operating conditions are satisfied. In the method of Kasaba [9], The x-axis is the time of the 20-minute period.

speed sensor data, respectively. The system detects a stop based on the wheel speed sensor and estimates the road-to-IMU pitch angle when the operating conditions are met. The vehicle was stopped 14 times by traffic signals, including the start point. In order to change the road-to-IMU pitch angle, an experiment was conducted with two load conditions of case (1) and case (2) of Fig. 20.

Mean error results in the Table. 2 compare the accuracy of the proposed algorithm with other algorithms under two load conditions. The proposed algorithm shows better accurate performance than other algorithms. In the case of the Kasaba [9] algorithm, the road slope angle is not considered. On a common road where ramps exist, the proposed algorithm shows better performance.

The results in Fig. 26 represent the precision performance of the proposed algorithm. Kasaba [9] algorithm, which estimates based on the direction of acceleration, requires a lot of data to converge and also requires that the average road slope in the data should be 0%. The proposed method robustly estimates the road-to-IMU pitch angle precisely and accurately in various road slopes and loading conditions.

VI. CONCLUSION

This paper proposed a system for estimating the road-to-headlamp pitch angle using an IMU sensor for automatic headlamp leveling. Instead of using an expensive height sensor, a low-cost IMU sensor and wheel speed sensor are used. The proposed estimation model used the assumption that the vehicle should follow the road slope direction. The proposed system is verified in three steps.

1) First, in the simulation, the effects of high-frequency noise and accelerometer bias on IMU pitch angle, road slope angle, and IMU pitch angle estimation system were analyzed. The bias of the accelerometer produced biased errors in the IMU pitch angle and road slope angle but did not significantly affect the road-to-IMU pitch angle. However, the high-frequency noise of the accelerometer causes a random walk by integration, causing the estimation variance. Based on the noise density specification of low- cost IMU, $300\mu g/\sqrt{Hz}$, a variance of 0.2° inevitably occurs when estimating the road slope.
2) Second, in the test road experiment, The IMU was attached to the actual vehicle, and the proposed system was verified in the various experiment environments. As with the simulation results, it was verified that the estimated variance of the road-to-IMU pitch angle was estimated to be within 0.2°. However, unlike simulations, the increased pitch motion during rapid acceleration resulted in an estimated variance increase of more than 0.2°.
3) Finally, precise estimation performance and stable convergence performance were verified in the common road when compared with other methods. In addition, the mean error of the proposed method is less than 0.2 degrees, exceeding the current UNECE regulations.

The proposed algorithm estimates only the static road-to-headlamp pitch angle. In future work, the author plans to develop an algorithm to estimate the dynamic road-to-headlamp pitch angle for dynamic headlamp leveling using only the IMU.

REFERENCES

[1] (2014). *Unece Regulation, no 48*. [Online]. Available: https://unece.org/fileadmin/DAM/trans/main/wp29/wp29regs/2015/R048r12e.pdf

[2] H. Zheng, H. Zhang, S. Xu, P. Wang, X. Yan, W. Zhao, and B. Wu, "An automatic headlamp leveling system based on the vehicle acceleration information," in *Proc. IEEE 6th Adv. Inf. Technol., Electron. Autom. Control Conf. (IAEAC)*, Oct. 2022, pp. 534–537.

[3] W. Zhao, H. Yang, C. Song, Y. Deng, B. Wu, X. Wang, and G. Lu, "An automatic headlamp leveling system based on the ramp detecting," in *Proc. IEEE 5th Adv. Inf. Technol., Electron. Autom. Control Conf. (IAEAC)*, Mar. 2021, pp. 1138–1141.

[4] S. E. Khadri, X. Moreau, A. Benine-Neto, M. Chevrié, W. M. Gonçalves, and F. Guillemard, "Design of the CRONE automatic headlight leveling system," *IFAC-PapersOnLine*, vol. 55, no. 27, pp. 208–213, 2022.

[5] S. V. Bayona, H. Koulouh, A. Noronha, F. Lamarque, and C. Prelle, "Novel use of a piezoelectric ultrasonic motor for headlamp leveling," in *Proc. IEEE/ASME Int. Conf. Adv. Intell. Mechatronics (AIM)*, Jul. 2019, pp. 1299–1304.

[6] A. Toda, "Vehicle headlamp leveling device," U.S. Patent 6 430 521, Aug. 6, 2002.

[7] H. Fechtner, M. Stenner, J. Schuster, T. Kliem, T. Teschner, and B. Schmuelling, "Automatic headlight leveling system with a modular design for the automotive aftermarket," in *Proc. IEEE 9th Int. Conf. Consum. Electron. (ICCE-Berlin)*, Sep. 2019, pp. 357–362.

[8] P. Nilsson, "Automatic headlight levelling using inertial sensors," Tech. Rep., 2017.

[9] Y. Kasaba, "An auto-leveling system using an acceleration sensor," in *Proc. 11th Int. Symp. Automot. Lighting (ISAL). Int. Symp. Automot. Lighting (ISAL)*, Sep. 2015, pp. 28–30.

[10] M. Mousa, K. Sharma, and C. G. Claudel, "Inertial measurement units-based probe vehicles: Automatic calibration, trajectory estimation, and context detection," *IEEE Trans. Intell. Transp. Syst.*, vol. 19, no. 10, pp. 3133–3143, Oct. 2018.

[11] W. He and J. Xi, "A quaternion unscented Kalman filter for road grade estimation," in *Proc. IEEE Intell. Vehicles Symp. (IV)*, Oct. 2020, pp. 1635–1640.

[12] J. Jauch, J. Masino, T. Staiger, and F. Gauterin, "Road grade estimation with vehicle-based inertial measurement unit and orientation filter," *IEEE Sensors J.*, vol. 18, no. 2, pp. 781–789, Jan. 2018.

[13] V. Winstead and I. V. Kolmanovsky, "Estimation of road grade and vehicle mass via model predictive control," in *Proc. IEEE Conf. Control Appl. (CCA)*, Aug. 2005, pp. 1588–1593.

[14] E. Raffone, "Road slope and vehicle mass estimation for light commercial vehicle using linear Kalman filter and RLS with forgetting factor integrated approach," in *Proc. 16th Int. Conf. Inf. Fusion*, Jul. 2013, pp. 1167–1172.

[15] H. Rehbinder and X. Hu, "Drift-free attitude estimation for accelerated rigid bodies," *Automatica*, vol. 40, no. 4, pp. 653–659, Apr. 2004.

[16] T. Harada, H. Uchino, T. Mori, and T. Sato, "Portable absolute orientation estimation device with wireless network under accelerated situation," in *Proc. IEEE Int. Conf. Robot. Autom. (ICRA)*, Apr. 2004, pp. 1412–1417.

[17] A. M. Sabatini, "Quaternion-based extended Kalman filter for determining orientation by inertial and magnetic sensing," *IEEE Trans. Biomed. Eng.*, vol. 53, no. 7, pp. 1346–1356, Jul. 2006.

[18] J. K. Schiffmann, "Vehicle attitude angle estimator and method," U.S. Patent 6 67 631, Jan. 13, 2004.

[19] R. Zhang, H. Yang, F. Höflinger, and L. M. Reindl, "Adaptive zero velocity update based on velocity classification for pedestrian tracking," *IEEE Sensors J.*, vol. 17, no. 7, pp. 2137–2145, Apr. 2017.

[20] L. Xiaofang, M. Yuliang, X. Ling, C. Jiabin, and S. Chunlei, "Applications of zero-velocity detector and Kalman filter in zero velocity update for inertial navigation system," in *Proc. IEEE Chin. Guid., Navigat. Control Conf.*, Aug. 2014, pp. 1760–1763.

[21] A. Ramanandan, A. Chen, and J. A. Farrell, "Inertial navigation aiding by stationary updates," *IEEE Trans. Intell. Transp. Syst.*, vol. 13, no. 1, pp. 235–248, Mar. 2012.

[22] M. Euston, P. Coote, R. Mahony, J. Kim, and T. Hamel, "A complementary filter for attitude estimation of a fixed-wing UAV," in *Proc. IEEE/RSJ Int. Conf. Intell. Robots Syst.*, Sep. 2008, pp. 340–345.

[23] J. K. Lee, E. J. Park, and S. N. Robinovitch, "Estimation of attitude and external acceleration using inertial sensor measurement during various dynamic conditions," *IEEE Trans. Instrum. Meas.*, vol. 61, no. 8, pp. 2262–2273, Aug. 2012.

[24] Z. Wu, D. Yuan, F. Zhang, and M. Yao, "Low-cost attitude estimation using GPS/IMU fusion aided by land vehicle model constraints and gravity-based angles," *IEEE Trans. Intell. Transp. Syst.*, vol. 23, no. 8, pp. 13386–13402, Aug. 2022.

[25] M. Kok, J. D. Hol, and T. B. Schön, "Using inertial sensors for position and orientation estimation," 2017, *arXiv:1704.06053*.

[26] D. Eberly, "Quaternion algebra and calculus," *Magic Softw. Inc*, vol. 26, pp. 1–8, Sep. 2002.

[27] H. Ahmed and M. Tahir, "Accurate attitude estimation of a moving land vehicle using low-cost MEMS IMU sensors," *IEEE Trans. Intell. Transp. Syst.*, vol. 18, no. 7, pp. 1723–1739, Jul. 2017.
[28] X. Yuan, S. Yu, S. Zhang, G. Wang, and S. Liu, "Quaternion-based unscented Kalman filter for accurate indoor heading estimation using wearable multi-sensor system," *Sensors*, vol. 15, no. 5, pp. 10872–10890, May 2015.
[29] J. Rohac, M. Sipos, and J. Simanek, "Calibration of low-cost triaxial inertial sensors," *IEEE Instrum. Meas. Mag.*, vol. 18, no. 6, pp. 32–38, Dec. 2015.

CHANSOO KIM received the B.S. degree in mechanical engineering from Konkuk University, Seoul, South Korea, in 2021, where he is currently pursuing the integrated master's degree with the Automotive Intelligence Laboratory. His research interest includes applications for sensor calibration for an autonomous vehicle.

JIWON SEOK received the B.S. degree in mechanical engineering from Konkuk University, Seoul, South Korea, in 2020, where he is currently pursuing the integrated master's and Ph.D. degree with the Automotive Intelligence Laboratory. His research interests include applications for localization, and mapping and sensor fusion for an autonomous vehicle.

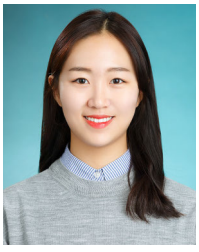

SOYEONG KIM received the B.S. and M.S. degrees in smart vehicle engineering from Konkuk University, Seoul, South Korea, in 2021 and 2022, respectively, where she is currently pursuing the Ph.D. degree with the Automotive Intelligence Laboratory. Her main research interests include applications for LiDAR processing, object tracking, localization, and mapping for an autonomous vehicles.

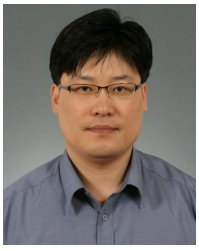

KUNHO LEE received the bachelor's degree in electrical engineering from the University of Ulsan, in 2001. From 2001 to 2005, he mass-produced the headlamp leveling actuator. From 2006 to 2010, he developed an adaptive front lighting system (AFLS) and mass-produced AFLS for LX and VF models. From 2020 to 2021, he researched leveling control system using inertial sensors with Konkuk University.

JONGHWA KIM received the master's degree in electronic engineering from Inha University, Incheon, in 2005. Since 2008, he has been a Software Engineer with the Lamp Laboratory, Hyundai Mobis Company.

INSUB MOON received the B.S. degree in electronic engineering from Inha University, Incheon, South Korea, in 2012. He has been a Software Engineer with the Headlamp Electronic Engineering Team, Hyundai Mobis Company, since 2012.

JISUNG KANG received the B.S. degree in electronic engineering from Sungkyunkwan University, Seoul, South Korea, in 2017. He is currently with the Headlamp Electronic Engineering Team, Hyundai Mobis Company. His research interest includes automotive embedded software.

KICHUN JO (Member, IEEE) received the B.S. degree in mechanical engineering and the Ph.D. degree in automotive engineering from Hanyang University, Seoul, South Korea, in 2008 and 2014, respectively. From 2014 to 2015, he was with the ACE Laboratory, Department of Automotive Engineering, Hanyang University, researching system design and implementation of autonomous cars. From 2015 to 2018, he was with the Valeo Driving Assistance Research, Bobigny, France, working on highly automated driving. He is currently an Assistant Professor with the Department of Smart Vehicle Engineering, Konkuk University, Seoul. His current research interests include localization and mapping, object tracking, information fusion, vehicle state estimation, behavior planning, and vehicle motion control for highly automated vehicles.